# Structure of the Rotor of the V-Type $Na^+$-ATPase from *Enterococcus hirae*

Takeshi Murata,[1] Ichiro Yamato,[2] Yoshimi Kakinuma,[3] Andrew G. W. Leslie,[4]* John E. Walker[1]*

The membrane rotor ring from the vacuolar-type (V-type) sodium ion–pumping adenosine triphosphatase ($Na^+$-ATPase) from *Enterococcus hirae* consists of 10 NtpK subunits, which are homologs of the 16-kilodalton and 8-kilodalton proteolipids found in other V-ATPases and in $F_1F_o$- or F-ATPases, respectively. Each NtpK subunit has four transmembrane α helices, with a sodium ion bound between helices 2 and 4 at a site buried deeply in the membrane that includes the essential residue glutamate-139. This site is probably connected to the membrane surface by two half-channels in subunit NtpI, against which the ring rotates. Symmetry mismatch between the rotor and catalytic domains appears to be an intrinsic feature of both V- and F-ATPases.

In eukaryotic cells, vital processes such as protein trafficking, endocytosis, neurotransmitter release, and intracellular pH regulation depend on the movement of ions across membranes by vacuolar adenosine triphosphatases (V-ATPases) (*1*), which are multisubunit complexes related to the $F_1F_o$- or F-ATPases found in eubacteria, mitochondria, and chloroplasts (*2*). Both classes have globular catalytic domains, $V_1$ and $F_1$, where ATP is hydrolyzed (and synthesized in F-ATPases), which are attached by central and peripheral stalks to the intrinsic membrane domains $V_o$ and $F_o$, where ions are pumped across the membrane. ATP hydrolysis generates rotation of both the central stalk and an attached membrane ring of hydrophobic subunits. Ions are pumped through a pathway in the interface between the rotating ring and a static membrane component, which is linked to the outside of the $V_1$ or $F_1$ domain by the peripheral stalk.

Eukaryotic V-ATPases contain 13 different polypeptides (*1*). Subunits A to H form the $V_1$ domain. Subunits A and B are the counterparts of subunits β and α, respectively, in the F-ATPases; three copies of each subunit are arranged around the central stalk, which is made of single copies of subunits D and F. The precise locations of the remaining subunits (C, E, G, and H) are uncertain, but they are thought to contribute to the peripheral stalk. The remaining subunits—a, c, c′, c″, and d—form $V_o$. The closely related c, c′, and c″ subunits are each composed of tandem homologous repeats of the sequences of F-type c subunits (*1*). The F-type subunits are folded into two transmembrane α helices that are linked by a loop oriented to the same side of the membrane as the $F_1$ domain (*3*, *4*). Their C-terminal α helices contain a conserved carboxylate side chain that is essential for ion transport (*5*). A carboxylate is also conserved in the equivalent position of helix 4 of the V-type subunits c and c′ (in the second repeat) but not in helix 2 (the first repeat). Subunit c″ has a fifth nonessential transmembrane α helix at its N terminus, and its essential glutamate is in helix 3 (*6*, *7*). In the V-ATPase from *Saccharomyces cerevisiae*, all three homologs are assembled into $V_o$ and are essential for a functional enzyme (*7*); and, like the c subunits in $F_o$, they probably form the $V_o$ rotary ring. V-ATPases also occur in prokaryotes; in *Enterococcus hirae*, a V-ATPase acts as a sodium ion extrusion pump (*8*). Its nine subunits are encoded in the $Na^+$-dependent triphosphatase (*ntp*) operon. Subunits A, B, D, and G make up the $V_1$ domain and are the homologs of subunits β, α, γ, and δ, respectively, in mitochondrial F-ATPases. Subunit C of V-ATPase has no counterpart in F-ATPase and may connect the foot of the central stalk to $V_o$, which is made of subunits K and I, the homologs of the F-ATPase subunits c and a, respectively. The K subunit (NtpK) is also the homolog of the eukaryotic V-type c subunits (Fig. 1A). Like the c subunits in eukaryotic V-ATPases, the sequence of NtpK contains tandem repeats in residues 1 to 79 and 80 to 156 with 22% identity and 44% similarity (Fig. 1B).

A surprising feature of F-ATPases is that the number of c protomers in the ring structures appears to vary between species. A complex of the $F_1$ domain with the c ring from the hydrogen ion–pumping $H^+$–F-ATPase from *S. cerevisiae* contains 10 c protomers (*4*). Isolated c rings from spinach chloroplasts consist of 14 c protomers (*9*), and rings from the sodium ion–pumping $Na^+$–F-ATPases from *Ilyobacter tartaricus* are made of 11 protomers (*10*). Biochemical and genetic evidence suggests that the $H^+$-ATPases in *Escherichia coli* and *Bacillus* PS3 have 10 protomers per c ring (*11*, *12*).

Here we describe the structure at 2.1 Å resolution of the K ring from *E. hirae*, which is the first high-resolution ring structure from either a V-type or an F-type enzyme.

**Structure of the K ring.** The structural data are summarized in Table 1. The 10 protomers of the K ring have very similar structures (Fig. 2); the root mean square deviation (RMSD) between α carbons is less than 0.06 and 0.08 Å for all atoms, except for crystal contact sites, where greater deviations occur. Each protomer is folded into five α helices, H0 to H4. H1 to H4 are transmembrane segments, and as expected from sequence homology, H1 and H2 resemble H3 and H4. The RMSD between all main-chain atoms in H1 and H2 (residues 11 to 46 and 51 to 79, respectively) compared with H3 and H4 (residues 87 to 122 and 127 to 155, respectively) is 1.0 Å. The 40 transmembrane α helices are packed in two concentric rings. H1 and H3 alternate in the inner ring, and H2 and H4 alternate in the outer ring. H1 and H3 (36 and 40 amino acids, respectively) are considerably longer than H2 and H4 (29 and 30 residues, respectively). H1 is linked to H2 and H3 to H4 by loop regions (residues 47 to 50 and 125 to 126, respectively), which, by analogy with F-ATPases, would lie proximal to the central-stalk region in the intact enzyme on the cytoplasmic side of the membrane. Another short loop (residues 80 to 84) links H2 and H3 on the periplasmic side of $V_o$ in the intact enzyme. H0 (residues 1 to 8) also lies distal from $V_1$. It points inward and slightly upward at 61° to the axis of H1 toward the center of the ring. H2 is kinked around $Pro^{62}$ and $Gly^{63}$, and H4 bends in the region of $Met^{137}$ and $Val^{138}$. The lower parts of H2 and H4 bend outward from the axis of the ring to approximately the same extent, as do the upper parts (mean values 11° and 26°, respectively); the bends in H1 and H3 are less pronounced. The effect of these curvatures is

[1]The Medical Research Council Dunn Human Nutrition Unit, Hills Road, Cambridge CB2 2XY, UK. [2]Department of Biological Science and Technology, Tokyo University of Science, Chiba, 278-8510, Japan. [3]Faculty of Agriculture, Ehime University, Matsuyama 790-8566, Japan. [4]The Medical Research Council Laboratory of Molecular Biology, Hills Road, Cambridge CB2 2QH, UK.

*To whom correspondence should be addressed. E-mail: walker@mrc-dunn.cam.ac.uk (J.E.W.); andrew@mrc-lmb.cam.ac.uk (A.G.W.L.)

to widen the upper and lower parts of the ring relative to the central region, especially on the cytoplasmic side (external and internal diameters of 83 and 54 Å, respectively). On the opposite side of the membrane, the inward-pointing H0 regions narrow the internal diameter of the ring to 29 Å.

The height of the K ring (68 Å) is similar to that of the c rings from the F-ATPases from *S. cerevisiae* (58 Å) (*4*) and *I. tartaricus* (70 Å) (*10*). These similarities arise from the relationships between the sequences of the tandem repeats in subunit K with the sequence of the c subunit (Fig. 1B). For example, the first K repeat and the *S. cerevisiae* c subunit are 45% similar and 17% identical, respectively, and the second K repeat and c subunit are 52% similar and 25% identical, respectively. However, these similarities in sequence and structure of the V- and F-type protomers notwithstanding, their ring diameters differ greatly, and the V-type ring is much larger than the F-type ring (external and internal diameters at the top of the F-type ring in *S. cerevisiae* are 55 and 27 Å, respectively, and in *I. tartaricus*, the values are 50 and 17 Å; the corresponding values in the K ring are 83 and 54 Å) (fig. S1). These differences in diameter probably reflect significant differences in the association of the ring with the foot of the central stalk. In F-ATPases, the interaction between the ring and the central stalk subunits (γ, δ, and ε in the mitochondrial enzyme) is direct (*4*). In bacterial V-type enzymes, the C subunit is thought to be interposed between the equivalent central stalk subunits and the ring (*13*) (in eukaryotic V-ATPases, the homolog of bacterial subunit C is subunit d and not subunit C).

**The $Na^+$-binding sites.** In each NtpK subunit, a strong peak of density between H2 and H4 adjacent to the γ carboxylate of $Glu^{139}$ was interpreted as a sodium ion. Other metal cations were also considered (Ca, Mg, Mn, Fe, Cu, Zn, and K), but $Na^+$ was the only metal cation in the crystallization medium, and it fit the coordination geometry best (*14*). Sodium ions bind to the *E. hirae* V-ATPase with high affinity (*15*). Each sodium ion is surrounded by five oxygen atoms 2.2 to 2.3 Å distant, four of them in the side chains of $Thr^{64}$, $Gln^{65}$, $Gln^{110}$, and $Glu^{139}$ (Fig. 3A), and the fifth in the main-chain carbonyl of $Leu^{61}$. Thus, residues in H2, H3, and H4 all contribute to the $Na^+$-binding pocket (Fig. 3). The bound sodium ions are occluded by the side chain of $Glu^{139}$, and the position of its γ carboxylate is stabilized by hydrogen bonds with the side chains of $Gln^{110}$, $Tyr^{68}$, and $Thr^{64}$ (Fig. 3A). Access to the bound ion to allow its exchange with the bulk phase (via a half-channel in subunit I, see below) can be achieved by changing the torsion angles of the side chain of $Glu^{139}$ without causing steric hindrance (Fig. 3C), although additional movements of adjacent side chains may also be necessary. Residues above and below the $Na^+$-binding site are all hydrophobic, and there is no plausible intrinsic channel within the K ring itself to provide access to the binding site from either the cytoplasm or the periplasm.

**Bound phospholipid, detergent, and water molecules.** After the 10 NtpK protomers had been fitted into the electron density, many peaks of positive density around the ring remained uninterpreted. Twenty of them lying close to the inside surface are bifurcated, which suggests that they arise from the acyl side chains of phospholipids. They are dis-

**Table 1.** Data collection and crystallographic analysis. Values in parentheses indicate the highest resolution shell. The overall figure of merit (after density modification) is 0.247 (0.458).

| Data set | Native 1 | Native 2 | $K_2PtCl_4$ | $K_2PtCl_6$ | $KAuCl_4$ |
|---|---|---|---|---|---|
| Wavelength (Å) | 0. 9792 | 0. 9792 | 1. 072 | 1.072 | 1.0397 |
| Resolution range (Å) | 61.3–2.10 | 67.4–2.30 | 87.7–2.80 | 67.4–3.20 | 67.4–2.90 |
| $R_{merge}$ (%)* | 9.1 (54.5) | 7.1 (52.5) | 10.0 (69.8) | 17.0 (70.6) | 9.1 (42.8) |
| Completeness (%) | 99.4 (97.5) | 88.4 (64.0) | 99.9 (99.8) | 98.8 (93.3) | 97.9 (86.8) |
| Unique observations | 184,567 | 124,148 | 78,994 | 48,674 | 69,975 |
| Redundancy | 3.7 (2.9) | 3.8 (3.1) | 13.7 (8.8) | 4.0 (4.0) | 4.4 (3.8) |
| $I/\sigma$ | 9.1 (1.8) | 12.1 (2.3) | 17.5 (2.9) | 7.1 (2.1) | 12.2 (2.7) |
| Wilson B factor ($Å^2$) | 32.3 | 44.9 | 72.1 | 88.8 | 76.4 |
| Phasing statistics | | | | | |
| Resolution range (Å) | | 20–2.30 | 20–3.0 | 20–3.5 | 20–3.0 |
| Number of heavy atom sites | - | - | 20 | 10 | 19 |
| $R_{cullis}$† (centric) | - | - | 0.653 | 0.907 | 0.899 |
| Phasing power‡ [iso/ano] | - | - | 1.40/1.120 | 0.70 | 0.59 |

*$R_{merge} = \Sigma_{hkl}\Sigma_i |I_i(hkl) - \langle I(hkl)\rangle| / \Sigma_{hkl}\Sigma_i I_i(hkl)$, where $h$, $k$, and $l$ are the Miller indices. †$R_{cullis} = \Sigma||F_{PH} - F_P| - F_H(calc)|/\Sigma|F_{PH} - F_P|$, where $F_H(calc)$ is the calculated heavy-atom structure factor. ‡Phasing power = $F_H(calc)/E$, where $E$ is phase-integrated lack of closure.

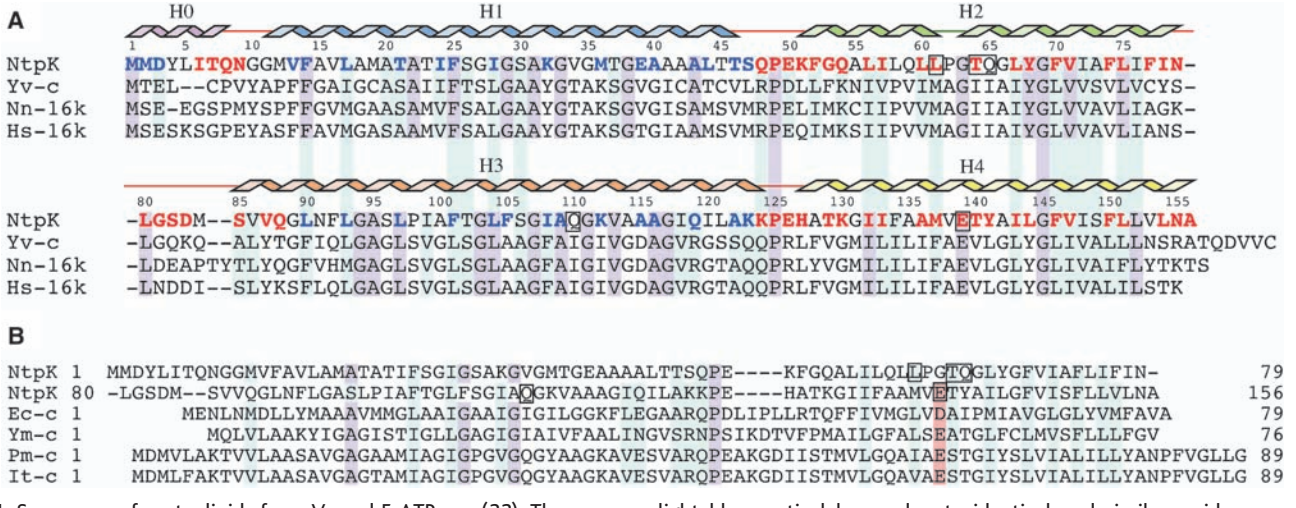


**Fig. 1.** Sequences of proteolipids from V- and F-ATPases (*32*). They were aligned with ClustalW (*33*). Dashes denote insertions. (**A**) The 16-kD proteolipids from V-ATPases from *E. hirae* (NtpK), the yeast vacuole (Yv-c), and human lysosomes (Hs-16k), and from gap junctions of *Nephrops norvegicus* (Nn-16k). The secondary structure, the positions of helices H0 to H4, and residue numbers of NtpK are shown above. Red and blue residues are exposed inside and outside the K ring, respectively. Violet and light blue vertical boxes denote identical and similar residues, respectively. (**B**) The tandem repeats of NtpK aligned with c subunits of F-ATPases from *E. coli* (Ec-c), yeast mitochondria (Ym-c), *P. modestum* (Pm-c), and *I. tartaricus* (It-c). The N- and C-terminal residues are numbered on the left and right, respectively. Residues with conserved essential side chains are shaded red. Amino acids forming the $Na^+$-binding site are boxed in (A) and (B).

tributed equally between the upper and lower regions of the model, with the openings of the bifurcation oriented downward in the upper layer and upward in the lower region, as expected in a phospholipid bilayer. The upper bifurcated moieties, but not the lower ones where the density is more limited, extend into regions of density that have been interpreted as phosphatidylglycerol (PG) head groups, because PG is the most abundant (57.1%) phospholipid head group in *E. hirae* (*16*). Because the most common fatty acyl chain in *E. hirae* phospholipids is $C_{16}$ (*17*), 10 1,2-dipalmitoyl-phosphatidylglycerol (DPPG) and 10 1,2-dipalmitoyl-glycerol (DPG) moieties were modeled into the upper and lower features, respectively (Fig. 4). The phosphate of the DPPG in the upper layer makes electrostatic interactions with $Lys^{32}$ in H1 ($O^5$-$N^{\varepsilon}$ distance 3.7 Å), and there is a hydrogen bond between $O^2$ in the glycerol moiety and $Lys^{32}$ of an adjacent protomer (distance 3.4 Å) (Fig. 4B). One of the DPPG acyl chains interacts with H1 via the side chains of $Leu^{17}$, $Thr^{21}$, and $Phe^{25}$, and with H3 via the side chain of $Phe^{101}$ in the adjacent protomer. The other DPPG acyl chain interacts with H1 via $Phe^{25}$ and with H3 via the side chains of $Phe^{101}$ and $Phe^{105}$ (listed side chains have a buried surface area >15 $Å^2$). The glycerol $O^9$ of DPG in the lower layer forms a hydrogen bond with the main chain amido of $Met^2$ (distance 3.1 Å), and it also interacts with the α-amino group (distance 3.5 Å). One of its acyl chains binds to H0 via the side chain of $Met^1$ and binds to $Phe^{14}$ and $Leu^{17}$ in H1 of the adjacent protomer (to the left) and to $Leu^{97}$ of the protomer two to the left. The other acyl chain binds to $Met^1$ and $Met^2$ in H0; $Leu^{17}$ in H1; and $Leu^{90}$, $Leu^{93}$, and $Leu^{97}$ in the adjacent protomer to the left. The thickness of the internal hydrophobic region of the lipid bilayer (the separation between the lipid glycerol backbone region on the two sides of the membrane) is about 25 Å. In a lipid bilayer of di-(C16:0), this thickness is estimated to be about 26 Å (*18*).

Within the annulus of the bound phospholipid bilayer, additional regions of electron density are associated with the upper phospholipid leaflet but not the lower one. Thirty regions of elongated density were interpreted as acyl side chains ($C_5$ to $C_{10}$) in a second shell of phospholipids, although the possibility that they derive from detergent molecules cannot be excluded (Fig. 4, A and C). There was no significant electron density in the central part of the ring, which suggests that phospholipids in this region are mobile and disordered.

It is evident that all external bound phospholipids were lost during the isolation of K rings, because no bifurcated regions of density were associated with the outside of the ring. During crystallization, both dodecyl- and undecylmaltoside were present, and a number of features next to the external regions toward the top of H2 and H4 have been interpreted as detergent molecules. The maltose ring is resolved in two molecules at crystal contact sites (Fig. 4A), and they appear to be undecyl- rather than dodecylmaltosides, but it is not possible to be certain. Twenty additional elongated features at approximately the same distance from the top of the ring have been interpreted as undecyl moieties, but the maltose moieties are disordered (Fig. 4, A to D). The model also contains 348 water molecules (Fig. 4) (*16*).

**Coupling of the K ring and the central stalk.** In the $H^+$-V-ATPase from *Thermus thermophilus*, subunit C is thought to be at the foot of the central stalk (*13*). It is a pointed molecule made of 12 α helices surrounding a core of six additional α helices, all lying approximately parallel to a threefold axis of pseudosymmetry. It has been proposed that the tapered end of this bundle (diameter, 28 Å) penetrates 12 Å into the membrane ring (*13*). In *T. thermophilus*, the c protomers (subunit L) have two transmembrane α helices, similar to the F-type c subunits, and the ring was modeled as 12 protomers of the c monomer

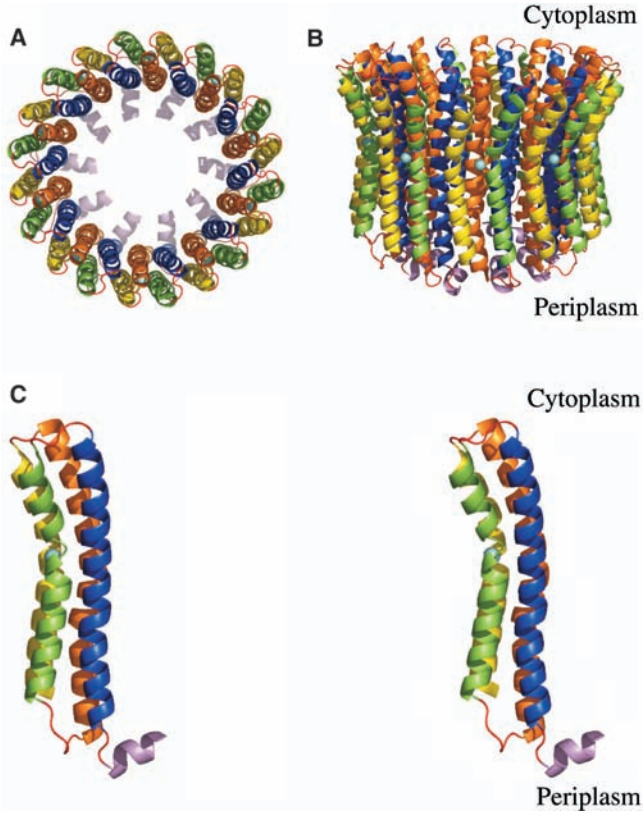


**Fig. 2.** Structure of the K ring. The ribbon representations are shown in mono (**A** and **B**) and in stereo (**C**). H0 (residues 1 to 8), H1 (11 to 46), H2 (51 to 79), H3 (85 to 124), H4 (127 to 156), and loops (9 to 10, 47 to 50, 80 to 84, and 125 to 126) are colored violet, blue, green, orange, yellow, and red, respectively. The $Na^+$ ions are shown as light blue spheres. (A) shows a view from the cytoplasmic side of the membrane; (B) and (C) show side views of the K ring and of the monomer, respectively. The cytoplasmic and periplasmic sides of the membrane are indicated.

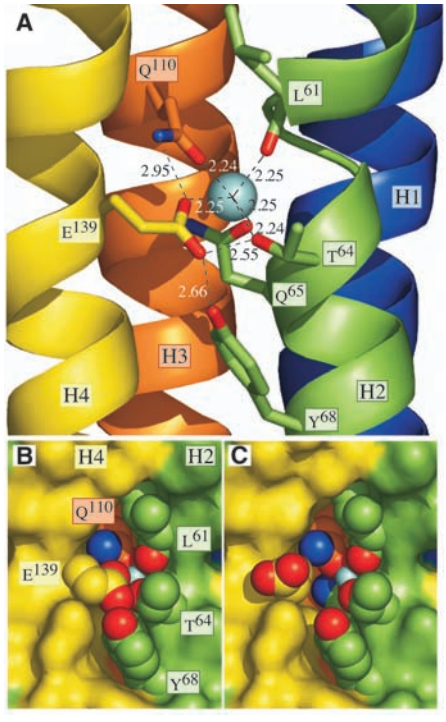


**Fig. 3.** The $Na^+$-binding pocket viewed from outside the K ring. The color code for helices H1 to H4 and the $Na^+$ ion is the same as in Fig. 2. Oxygen and nitrogen atoms are red and dark blue, respectively. Dotted lines are $Na^+$-O bonds and potential hydrogen bonds, with distances in Å. Residues involved in $Na^+$ binding are shown in stick (**A**) or space-filling (**B** and **C**) representation. In (B) and (C), the $Na^+$ ion is in light blue, and residues not involved in binding it are represented as the solvent-accessible surface. In (C), to open the $Na^+$-binding pocket, the torsion angles of the side chain of $Glu^{139}$ have been changed from (–170, 72), as determined in the structure, to (70, 170).

from *E. coli* F-ATPase determined by solution nuclear magnetic resonance (NMR) (*3*), giving a pore diameter of 30 Å, to act as a closely fitting socket for the 28 Å taper of subunit C. The sequence of NtpC is 20% identical and 40% similar to that of the C subunit of *T. thermophilus*, and it is likely to have a similar structure. The *T. thermophilus* C subunit structure was docked with the K ring, and, with the taper of subunit C penetrating into the central cavity almost to the narrowest region at the midpoint of the ring, it occupies most of the cavity, although some structural changes would be needed to achieve an extensive interaction (Fig. 4E). This model of the K ring with the C subunit differs substantially from the proposal (*13*) for the interaction of the C subunit with the c ring in *T. thermophilus*, where the smaller diameter of a ring assumed to be composed of 12 F-type c protomers restricts the penetration to the tip of the taper in subunit C.

**Sodium ion translocation.** Three key questions about the mechanism for transmembrane $Na^+$ translocation are as follows: (i) How does the outer surface of the ring interact with the phospholipid bilayer. (ii) What is the nature of the interactions of the ring with subunit I? (iii) To what extent is the $Na^+$-binding site accessible to the external milieu? Although no phospholipids are bound to the outer surface, their likely regions of interaction with the K ring can be inferred from features such as the distribution of charged and hydrophobic side chains and the locations of bound water molecules. In known structures of membrane proteins, tyrosine, asparagine, and lysine residues (and also arginine, histidine, tryptophan, and serine) are often found near phospholipid head groups, acting as primary ligands for phosphodiester groups, and additional stabilization sometimes comes from threonine and glutamine residues (*18*, *19*). The outside of the K ring has a hydrophobic belt 39 Å wide (Fig. 4D, α-carbon distance between $Lys^{130}$ and $Asn^{155}$) corresponding to the head-group separation in a lipid bilayer (*18*). This position for the lipid bilayer allows interactions between phosphodiester groups in the upper leaflet and the side chains of $Gln^{54}$, $Thr^{129}$, and $Lys^{130}$, and in the lower leaflet with $Asn^{79}$ and $Asn^{155}$. The distribution of bound water and detergent molecules supports this interpretation. This arrangement places the $Na^+$-binding site close to the center of the bilayer, as in the c ring in *I. tartaricus* (*10*). Although several polar residues involved in binding the $Na^+$ ion are exposed on the outer surface of the K ring, the network of hydrogen bonds surrounding the $Na^+$ site satisfies all potential hydrogen-bonding groups (Fig. 3A). With a bound $Na^+$, there is no energy penalty for these residues being near the center of the bilayer.

The position of the $Na^+$-binding site close to the middle of the lipid bilayer, and the absence of any intrinsic K-ring channel leading to the site, support a "two–half-channel" ion translocation model (Fig. 5) as proposed for F-ATPases (*20*). The clockwise rotation of the K ring, as viewed from the cytoplasm, brings an occupied $Na^+$-binding site into the K-ring–subunit-I interface. The proximity of the $Na^+$ site to NtpI-$Arg^{573}$, which is essential for ion transport (*21*), produces an electrostatic interaction between $Arg^{573}$ and $Glu^{139}$, disrupting the hydrogen-bond network and releasing the $Na^+$ ion into the periplasm via a half-channel in NtpI (the ion release may possibly be assisted by electrostatic repulsion by $R^{573}$). Further rotation, which may disrupt the Arg-Glu interaction, brings the site into contact with a second half-channel, resulting in the binding of a cytoplasmic $Na^+$ ion. With the site occupied, the energy barrier to further rotation is lowered, bringing the site beyond the I–K-ring interface. This model differs from an earlier one for the V-ATPase based on $Na^+$-exchange experiments in detergent (*8*, *15*) where a single channel connected the ion-binding site to the periplasm at the I–K-ring interface, giving free cytoplasmic access to most $Na^+$-binding sites. The earlier model is incompatible with the structure, and the kinetics of exchange (fast- and slow-exchange sites >1.7 and 0.16 $min^{-1}$, respectively) are much slower than physiological ion-pumping rates.

A "single channel" model of $Na^+$ translocation has also been proposed for the F-ATPase from *Propioniogenium modestum* (*22*), where the $Na^+$-binding site is placed close to the membrane center on the basis of biochemical evidence (*23*, *24*), but $Na^+$-exchange experiments have been interpreted as suggesting free cytoplasmic access to the sites (*25*). The observations were reconciled by proposing an intrinsic c-ring channel connecting the ion-binding sites to the cytoplasm (*10*, *23*, *2*).

In a three-dimensional model of the c ring of the $Na^+$-F-ATPase from *I. tartaricus* based

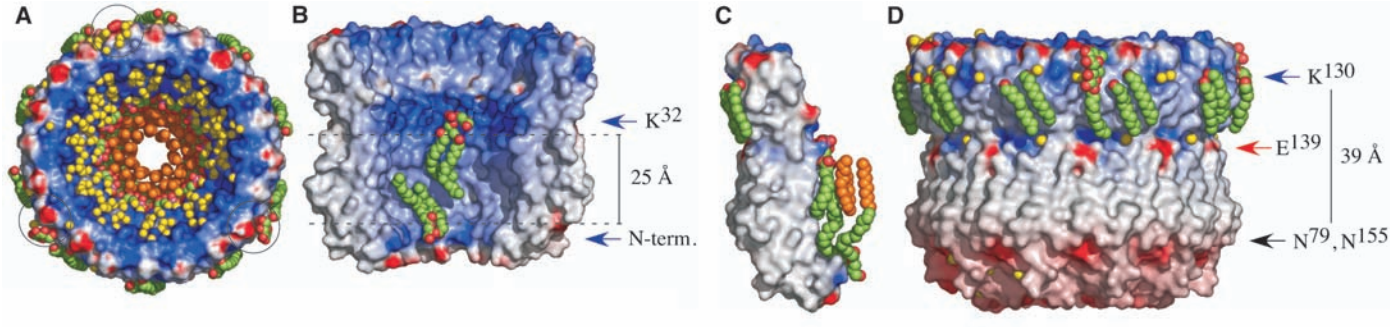


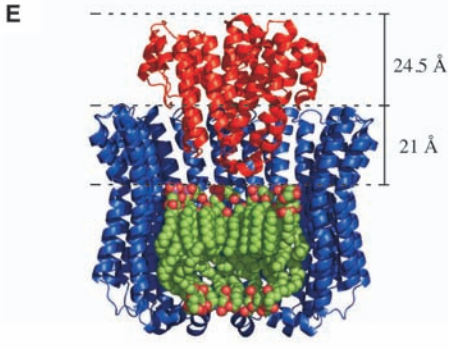


**Fig. 4.** Localization of lipid, detergent, and water molecules and interaction of the K ring with subunit C. The solvent-accessible surface of the K ring is colored according to the electrostatic potential (red, negative; blue, positive; gray, neutral). Lipids and detergents are shown in space-filling representation (C and O atoms are green and red, respectively). The C atoms of incomplete acyl chains from either lipid or detergent are orange. Yellow spheres are water molecules. (**A**) View from the cytoplasm. Three circles show crystal contacts. (**B**) Cut-away view showing the interior surface of one half of the ring and one pair of lipids in the bilayer inside the ring. Dashed lines show the location of the hydrophobic core of the lipid bilayer inside the ring, which is defined as the region between the lipid glycerol backbone moieties. (**C** and **D**) Side views, respectively, of the surface of the K monomer with lipids and detergent tails and of the outer surface of the whole ring with all resolved detergent and water molecules. In (D), the extent of the hydrophobic belt, 39 Å, is indicated by a vertical line. (**E**) Coupling of the K ring and the central stalk. The *T. thermophilus* subunit C (colored red, Protein Data Bank code 1r5z) (*13*) was docked manually into the K ring; one half of the K ring (blue) is shown with interior lipids (in space-filling representation; C and O atoms are green and red, respectively). The marked distances, 21 and 24.5 Å are, respectively, the depth of penetration of subunit C into the K ring and the extent to which subunit C protrudes from the ring and thus its contribution to the height of the central stalk.

on electron cryogenic microscopy (*10*), rods of density for the N- and C-terminal helices in an 11-fold ring and weaker connecting densities were observed, but side chains could not be identified. The model was constructed with a series of conserved glycines (residues 27, 29, 31, and 33) facing neighboring subunits in the inner ring of helices, with $Gln^{32}$ (involved in $Na^+$ binding) facing the C-terminal helix to achieve the tight packing of the inner helices suggested by conservation of the glycines. There was less information to constrain the orientation of the C-terminal helix, but because both $Glu^{65}$ and $Ser^{66}$ are implicated in $Na^+$ binding (*26*), the face of the helix containing these residues was placed toward the N-terminal helix, allowing a chain of polar residues ($Gln^{61}$, $Thr^{56}$, $Ser^{55}$, $Asp^{52}$, and $Lys^{50}$) to connect the $Na^+$-binding site to the cytoplasm, providing free access to the $Na^+$-binding site.

To explore this proposal, a model of the *I. tartaricus* c ring based on the NtpK structure has been constructed (*16*). From this model, it appears that there is no intrinsic ion channel in the *I. tartaricus* ring. Thus, it is likely that $Na^+$ translocation in the F-ATPases from *I. tartaricus* and *P. modestum* also relies on two half-channels (in subunit a) rather than on a single periplasmic channel, and this feature is common to ion transport mechanisms in both F-and V-ATPases.

The overall fold of helices H3 and H4 of NtpK is very similar to the low-pH NMR structure of an *E. coli* c monomer (*3*). However, the position of the essential carboxylate ($Glu^{139}$ in NtpK and $Asp^{61}$ in *E. coli* subunit c) differs by almost half an α-helical turn, corresponding to a rotation around the axis of the helix of approximately 150°. In view of the sequence similarity and because $Asp^{61}$ is assumed to be protonated in the NMR structure so that the ion binding site is occupied in both proteins, this result is surprising. A more detailed comparison of the NtpK and c-ring models will be described elsewhere.

**Symmetry of rotor rings in V- and F-ATPases.** By single-particle averaging of the same preparation of K rings as used for crystallography, a sevenfold symmetry was observed (*27*), which is incompatible with the structure of the K ring. A proper explanation of this discrepancy has not yet been found, but the x-ray structure demonstrates the 10-fold symmetry unequivocally, and it is likely that this is the symmetry of the ring in the fully assembled V-ATPase. Also, given the close sequence relationship between K subunits and c subunits in other V-ATPases, the 10-fold symmetry of the K rings is likely to have wider significance for V-ATPases. On the basis of various strands of evidence, including chemical analysis (*28*) and electron microscopy (*29*), it has become accepted that the symmetry of V-type rings is sixfold. This situation is reminiscent of the history of c-ring stoichiometries in F-ATPases, where, on the basis of similar kinds of experimentation, it was thought that the c rings had 12-fold symmetry, until higher resolution structural information demonstrated clearly the 10-fold symmetry in the $F_1$-$c_{10}$ complex from the F-ATPase from *S. cerevisiae* (*4*) and 11-fold and 14-fold symmetries in rings isolated from the $Na^+$-ATPases from *I. tartaricus* (*10*) and the $H^+$-ATPase from spinach chloroplasts (*9*), respectively. Thus, the earlier sixfold symmetries of c rings from V-ATPases will require reevaluation by high-resolution structural methods.

The fundamental importance of the observed ring stoichiometries is twofold. First, the range of values suggests that not all species pay the same energetic price either to make an ATP molecule in the F-ATPases or to pump a proton or a sodium ion in V-ATPases and bacterial F-ATPases. According to extant models for ATP synthesis, each 360° rotation of the central stalk and the attached c ring generates three ATP molecules in the $F_1$ domain, and the generation of a 360° rotation requires each of the c subunits in the ring to translocate an ion. Thus, the number of protons (or sodium ions) required to make an ATP molecule in enzymes with c ring symmetries of 10, 14, and 11 will be 3.3, 4.7, and 3.7, respectively. Similarly, hydrolysis of an ATP molecule in the V-ATPase from *E. hirae* will be coupled to the outward translocation of 3.3 sodium ions. Second, the mismatch of symmetries between catalytic and membrane domains observed now in both F- and V-ATPases could be an important intrinsic feature of both enzyme types, helping to reduce potential-energy barriers to rotation that might otherwise exist in enzymes with matching symmetries (*4*). Symmetry mismatch is also a feature of the machinery for packaging DNA into bacteriophage heads (*30*) and of the bacterial flagellar motor (*31*). Like the F- and V- ATPases, both machines have a rotary action.

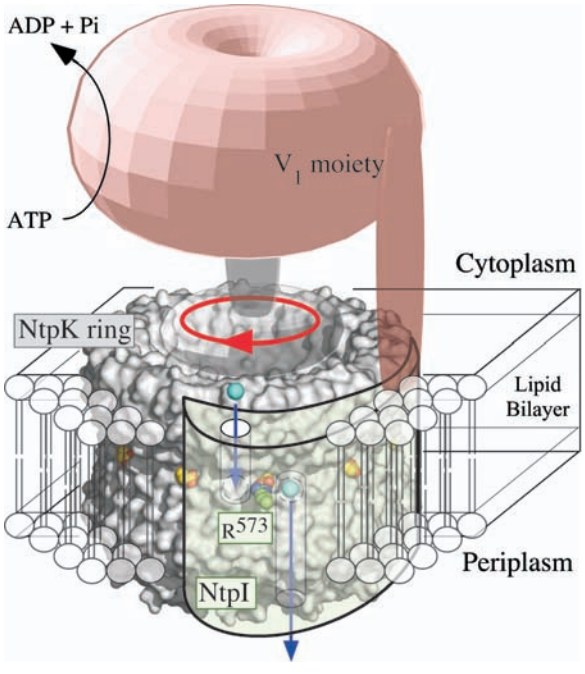


**Fig. 5.** A model for ion translocation by the V-ATPase of *E. hirae*. The model is based on the structure of the K ring, shown in space-filling representation with $Glu^{139}$ in yellow with red oxygen atoms. Subunit I (structure unknown) is green and in close proximity to the K ring in space-filling representation with the essential residue $Arg^{573}$ (*21*) in a half-channel connecting to the periplasm. Another half-channel links the ion-binding site to the cytoplasm ($Na^+$ ions are blue). Clockwise rotation of the ring (arrow) driven by ATP hydrolysis in $V_1$ transfers bound $Na^+$ ions, which have reached the ion-binding site via a half-channel connecting to the cytoplasm, to a position where they transfer to a second half-channel leading to the periplasm.

**References and Notes**


1. T. Nishi, M. Forgac, *Nat. Rev. Mol. Cell Biol.* **3**, 94 (2002).
2. J. E. Walker, *Angew. Chem. Int. Ed. Engl.* **37**, 2308 (1998).
3. M. E. Girvin, V. K. Rastogi, F. Abildgaard, J. L. Markley, R. H. Fillingame, *Biochemistry* **37**, 8817 (1998).
4. D. Stock, A. G. W. Leslie, J. E. Walker, *Science* **286**, 1700 (1999).
5. J. Hermolin, R. H. Fillingame, *J. Biol. Chem.* **264**, 3896 (1989).
6. T. Nishi, S. Kawasaki-Nishi, M. Forgac, *J. Biol. Chem.* **278**, 5821 (2003).
7. R. Hirata, L. A. Graham, A. Takatsuki, T. H. Stevens, Y. Anraku, *J. Biol. Chem.* **272**, 4795 (1997).
8. T. Murata, M. Kawano, K. Igarashi, I. Yamato, Y. Kakinuma, *Biochim. Biophys. Acta* **1505**, 75 (2001).
9. H. Seelert *et al.*, *Nature* **405**, 418 (2000).
10. J. Vonck *et al.*, *J. Mol. Biol.* **321**, 307 (2002).
11. W. Jiang, J. Hermolin, R. H. Fillingame, *Proc. Natl. Acad. Sci. U.S.A.* **98**, 4966 (2001).
12. N. Mitome, T. Suzuki, S. Hayashi, M. Yoshida, *Proc. Natl. Acad. Sci. U.S.A.* **101**, 12159 (2004).
13. M. Iwata *et al.*, *Proc. Natl. Acad. Sci. U.S.A.* **101**, 59 (2004).
14. M. M. Harding, *Acta Crystallogr.* **D58**, 872 (2002).
15. T. Murata, K. Igarashi, Y. Kakinuma, I. Yamato, *J. Biol. Chem.* **275**, 13415 (2000).
16. Materials and methods are available as supporting material on *Science* Online.
17. F. A. Ibbott, A. Abrams, *Biochemistry* **19**, 2008 (1964).
18. A. G. Lee, *Biochim. Biophys. Acta* **1612**, 1 (2003).
19. H. Palsdottir, C. Hunte, *Biochim. Biophys. Acta* **1666**, 2 (2004).
20. W. Junge, H. Lill, S. Engelbrecht, *Trends Biochem. Sci.* **22**, 420 (1997).
21. M. Kawano, K. Igarashi, I. Yamato, Y. Kakinuma, *J. Biol. Chem.* **277**, 24405 (2002).
22. G. Kaim, U. Matthey, P. Dimroth, *EMBO J.* **17**, 688 (1998).
23. C. von Ballmoos *et al.*, *J. Biol. Chem.* **277**, 3504 (2002).
24. C. von Ballmoos, T. Meier, P. Dimroth, *Eur. J. Biochem.* **269**, 5581 (2002).
25. G. Kaim, P. Dimroth, *EMBO J.* **17**, 5887 (1998).

26. G. Kaim, F. Wehrle, U. Gerike, P. Dimroth, *Biochemistry* **36**, 9185 (1997).
27. T. Murata *et al.*, *J. Biol. Chem.* **278**, 21162 (2003).
28. H. Arai *et al.*, *J. Biol. Chem.* **263**, 8796 (1999).
29. A. Holzenburg *et al.*, *Eur. J. Biochem.* **213**, 21 (1993).
30. R. W. Hendrix, *Proc. Natl. Acad. Sci. U.S.A.* **75**, 4779 (1978).
31. D. R. Thomas, D. G. Morgan, D. J. DeRosier, *Proc. Natl. Acad. Sci. U.S.A.* **96**, 10134 (1999).
32. Single-letter abbreviations for the amino acid residues are as follows: A, Ala; C, Cys; D, Asp; E, Glu; F, Phe; G, Gly; H, His; I, Ile; K, Lys; L, Leu; M, Met; N, Asn; P, Pro; Q, Gln; R, Arg; S, Ser; T, Thr; V, Val; W, Trp; and Y, Tyr.
33. J. D. Thompson, D. G. Higgins, T. J. Gibson, *Nucleic Acids Res.* **22**, 4673 (1994).
34. This work was supported by the Medical Research Council. T.M. was supported partly by a Fellowship for Research Abroad from the Japan Society for the Promotion of Science. We thank the staff at the European Synchrotron Radiation Facility in Grenoble for their help. Coordinates and structure factors (accession codes 2bl2 and r2bl2sf) have been deposited in the Protein Data Bank.

**Supporting Online Material**
www.sciencemag.org/cgi/content/full/1110064/DC1
Materials and Methods
SOM Text
Fig. S1
References

21 January 2005; accepted 8 March 2005
Published online 31 March 2005;
10.1126/science.1110064
Include this information when citing this paper.

# Structure of the Rotor Ring of F-Type $Na^+$-ATPase from *Ilyobacter tartaricus*

**Thomas Meier,[1] Patrick Polzer,[2] Kay Diederichs,[2]* Wolfram Welte,[2] Peter Dimroth[1]***

**In the crystal structure of the membrane-embedded rotor ring of the sodium ion–translocating adenosine 5′-triphosphate (ATP) synthase of *Ilyobacter tartaricus* at 2.4 angstrom resolution, 11 c subunits are assembled into an hourglass-shaped cylinder with 11-fold symmetry. Sodium ions are bound in a locked conformation close to the outer surface of the cylinder near the middle of the membrane. The structure supports an ion-translocation mechanism in the intact ATP synthase in which the binding site converts from the locked conformation into one that opens toward subunit a as the rotor ring moves through the subunit a/c interface.**

In the $F_1F_o$ ATP synthase, the cytoplasmic $F_1$ catalytic domain (subunits $\alpha_3\beta_3\gamma\delta\varepsilon$) is linked by means of a central and a peripheral stalk (subunits $\gamma/\varepsilon$ and $b_2/\delta$, respectively) to the intrinsic membrane domain called $F_o$ (subunits $ab_2c_{10\text{-}14}$). Each of these domains functions as a reversible rotary motor and exchanges energy with the opposite motor by mechanical rotation of the central stalk. During ATP synthesis, energy stored in an electrochemical gradient of protons or $Na^+$ ions fuels the $F_o$ motor, which causes the stalk to rotate with the inherently asymmetric $\gamma$ subunit acting as a camshaft to continuously change the conformation of each catalytic $\beta$ subunit. These sequential interconversions, which result in ATP synthesis, endow the binding sites with different nucleotide affinities [for reviews see (*1*–*3*)]. The rotational model, which explains a wealth of biochemical and kinetic data, is impressively supported by the crystal structure of $F_1$ (*4*) and was experimentally verified by biochemical, spectroscopic, and microscopic techniques (*5*).

The $F_o$ motor consists of an oligomeric ring of c subunits that is abutted laterally by the a and $b_2$ subunits (*6*). The c ring, together with $\gamma/\varepsilon$ subunits, forms the rotor assembly, which spins against the stator components $ab_2\delta\alpha_3\beta_3$. Ion translocation at the interface between subunit a and the c ring, driven by the ion motive force, is thought to generate torque (*7*–*10*) applied to the $\gamma$ subunit, which is then used to promote the conformational changes required for ATP synthesis at the $F_1$ catalytic sites.

Despite intense efforts, little is known about the structural details of $F_o$. This lack of information hinders our understanding of how this molecular motor functions. The nuclear magnetic resonance (NMR) structures of the c monomer of *Escherichia coli* (*7*, *11*) showed that the protein is folded into two $\alpha$ helices linked by a loop. Other structural studies indicated that the c subunits of the oligomer are tightly packed into two concentric rings of helices (*12*, *13*). The number of c monomers per ring varies between $n$ = 10, 11, and 14 units in the ATP synthases from yeast (*12*), *I. tartaricus* (*13*), and spinach chloroplasts (*14*), respectively.

**Structure of the c ring.** We chose to determine the crystal structure of the *I. tartaricus* c ring because of its inherent stability and relative ease of isolation (*15*). After purification and crystallization of wild-type c ring (*16*), the structure was solved (table S1) by molecular replacement (*17*) using a medium-resolution (6 Å) c-ring backbone model derived from electron crystallography (*13*). The asymmetric unit of the crystal contains 4 c rings. These rings are arranged in two parallel, but laterally translated, c-ring dimers each formed by a coaxial association of two rings that interact with their termini in a tail-to-tail fashion. A non-crystallographic symmetry restraint was imposed during refinement at 2.4 Å over the 44 monomers in the asymmetric unit (3916 residues) with the exclusion of the loop regions that form crystal contacts, which substantially improved the electron density and resulted in an atomic model without Ramachandran plot outliers.

The electron density map of a single c ring shows a cylindrical, hourglass-shaped protein complex of ~70 Å in height, and with an outer diameter of ~40 Å in the middle and ~50 Å at the top and bottom. Eleven c subunits, each composed of two membrane-spanning $\alpha$ helices forming a hairpin, are arranged around an 11-fold axis, creating a tightly packed inner ring with their N-terminal helices (Fig. 1). The C-terminal helices pack into the grooves formed between N-terminal helices, producing an outer ring, in agreement with previous medium-resolution structures (*12*, *13*). In the electron density map, the backbone and side chains of all amino acids are clearly defined, except for the C-terminal glycine. The N- and C-terminal helices are connected by a loop formed by the highly conserved peptide $Arg^{45}$, $Gln^{46}$, and $Pro^{47}$, which is exposed to the cytoplasmic surface (Fig. 2) (*18*, *19*). The chain termini are exposed to the periplasm.

The C-terminal helices are shorter than the N-terminal helices, owing to a break at $Tyr^{80}$ followed by another short helix of one turn (Figs. 1 and 2). For each helix, an individual plane can be found that roughly contains the axis of the helix and the c-ring symmetry axis (Fig. 1A). All helices show a bend of about 20° in the middle of the membrane (at $Pro^{28}$ and $Glu^{65}$ in the N-terminal and the C-terminal helices, respectively), causing the narrow part of the hourglass shape. Moreover, the bend tilts the helices in the cytoplasmic half out of the plane by ~10°, yielding a right-handed twisted packing (Fig. 1A). When the c ring is viewed from the cytoplasm, it rotates counterclockwise during ATP synthesis (*20*) against the drag imposed by the $F_1$ motor components. Thus, the resulting torque might decrease the bend and increase the interhelical distance in the cytoplasmic part of the c ring, depending on the energies involved. Such a conformational change under load might serve to store elastic energy in the c ring, adding to that described for the central and peripheral stalk subunits (*21*). A change in the twist of the helices is supported by calculations (*22*) that show in the lowest-order mode a torsional

[1]Institut für Mikrobiologie, Eidgenössische Technische Hochschule (ETH), Zürich Hönggerberg, Wolfgang-Pauli-Str. 10, CH-8093 Zürich, Switzerland. [2]Fachbereich Biologie, Universität Konstanz M656, D-78457 Konstanz, Germany.

*To whom correspondence should be addressed. E-mail: dimroth@micro.biol.ethz.ch (P.D.); kay.diederichs@uni-konstanz.de (K.D.)